The Astrophysical Journal, 727:95 (13pp), 2011 February 1 doi:10.1088/0004-637X/727/2/95

BLACK HOLE–NEUTRON STAR MERGERS AND SHORT GAMMA-RAY BURSTS: A RELATIVISTIC TOY MODEL TO ESTIMATE THE MASS OF THE TORUS

Francesco Pannarale[1], Aaryn Tonita[1], and Luciano Rezzolla[1,2]
[1] Max-Planck-Institut für Gravitationsphysik, Albert Einstein Institut, Am Muehlenberg 1, D-14476, Potsdam, Germany;
francesco.pannarale@aei.mpg.de, aaryn.tonita@aei.mpg.de, luciano.rezzolla@aei.mpg.de
[2] Department of Physics and Astronomy, Louisiana State University, 202 Nicholson Hall, Tower Drive Baton Rouge, LA 70803-4001, USA
Received 2010 July 23; accepted 2010 November 2; published 2011 January 10

ABSTRACT

The merger of a binary system composed of a black hole (BH) and a neutron star (NS) may leave behind a torus of hot, dense matter orbiting around the BH. While numerical-relativity simulations are necessary to simulate this process accurately, they are also computationally expensive and unable at present to cover the large space of possible parameters, which include the relative mass ratio, the stellar compactness, and the BH spin. To mitigate this and provide a first reasonable coverage of the space of parameters, we have developed a method for estimating the mass of the remnant torus from BH–NS mergers. The toy model makes use of an improved relativistic affine model to describe the tidal deformations of an extended tri-axial ellipsoid orbiting around a Kerr BH and measures the mass of the remnant torus by considering which of the fluid particles composing the star are on bound orbits at the time of the tidal disruption. We tune the toy model by using the results of fully general-relativistic simulations obtaining relative precisions of a few percent and use it to investigate the space of parameters extensively. In this way, we find that the torus mass is largest for systems with highly spinning BHs, small stellar compactnesses, and large mass ratios. As an example, tori as massive as $M_{b,\rm tor} \simeq 1.33\,M_\odot$ can be produced for a very extended star with compactness $C \simeq 0.1$ inspiralling around a BH with dimensionless spin parameter $a = 0.85$ and mass ratio $q \simeq 0.3$. However, for a more astrophysically reasonable mass ratio $q \simeq 0.14$ and a canonical value of the stellar compactness $C \simeq 0.145$, the toy model sets a considerably smaller upper limit of $M_{b,\rm tor} \lesssim 0.34\,M_\odot$.

Key words: black hole physics – gamma-ray burst: general – stars: neutron

Online-only material: color figures

1. INTRODUCTION

The most widely accepted scenario to explain the phenomenology associated with short-hard gamma-ray bursts (SGRBs) involves the merger of either black hole (BH)–neutron star (NS) systems or of binary NS systems (Nakar 2007). In either case, the remnant consists of a BH with negligible baryon contamination along its polar symmetry axis and of a hot, massive accretion torus surrounding it, which releases energy as it accretes onto the BH, typically in the form of a relativistic jet. With these fundamental ingredients of the standard SGRB model, an intense neutrino flux is emitted as the torus accretes onto the BH, triggering a high-entropy gas outflow off the surface of the accretion torus, i.e., "neutrino wind." At the same time, energy deposition by $\nu\bar{\nu}$ annihilation in the baryon-free funnel around the BH rotation axis powers relativistically expanding $e^{\pm}$ jets, which can give rise to the observed GRB emission. Other burst mechanisms have, of course, been proposed; since these principally involve magnetically launched jets and since we do not address magnetic fields in this paper, we have briefly summarized only the burst mechanism powered by neutrino annihilation; the interested reader may refer to Lee & Ramirez-Ruiz (2007) for a thorough review.

The simulation of these events "ab initio" requires an adequate description of general relativity, relativistic (magneto)hydrodynamics, and a proper microphysical equation of state (EOS). Typically, the only way to model these systems accurately is to resort to numerical-relativity simulations, solving consistently both the Einstein equations and those of relativistic hydrodynamics or magnetohydrodynamics. These simulations have made considerable progress in the last few years (see, for instance, Oechslin & Janka 2007; Anderson et al. 2008a; Anderson et al. 2008b; Baiotti et al. 2008; Yamamoto et al. 2008; Liu et al. 2008; Giacomazzo et al. 2009; Rezzolla et al. 2010; Bauswein et al. 2010 for recent studies of NS–NS binaries or Kluzniak & Lee 1999; Rosswog 2005; Löffler et al. 2006; Etienne et al. 2008; Shibata & Taniguchi 2008; Duez et al. 2010; Etienne et al. 2009; Duez et al. 2008; Shibata et al. 2009; Chawla et al. 2010 for corresponding work on BH–NS binaries). Despite the fact that this type of simulations is now possible, they remain nevertheless both challenging and computationally intensive. Numerical simulations of NS–NS mergers have now reached a rather high level of accuracy (see Baiotti et al. 2009 and the discussion in the appendix of Rezzolla et al. 2010), and different codes have been shown to yield results that agree to 10% (at worse) when using the same initial data (Baiotti et al. 2010). However, the situation is much more uncertain in the case of BH–NS binaries, for which no direct comparison among different codes has been made yet and the results of the simulations from different codes are sometimes not in agreement. As an example, the merger of the same binary with mass ratio 1/3 yields a torus with a baryonic mass which is ∼4% of the NS in Etienne et al. (2009) and $\lesssim 0.001\%$ in Shibata et al. (2009). As a result, no reliable knowledge is available at the moment on how the mass of the torus depends on the most important parameters of the system: the mass ratio, the stellar compactness, and the BH spin.

These problems, along with the need of a better understanding of the tidal-disruption process, have pushed the parallel development of pseudo-Newtonian BH–NS calculations—e.g., Ruffert & Janka (2010) use the Paczyński–Wiita phenomenological potential to mimic the innermost stable circular orbit (ISCO) of the

BH in a Newtonian setting—and of semi-analytical approaches to the problem. Regarding the latter, Shibata (1996), for instance, described the necessary conditions for the production of an accretion torus of appreciable size by requiring that the NS disruption occurs at a tidal radius $r_{\rm tide}$ that is larger than the ISCO of the BH $r_{\rm ISCO}$. Unfortunately, Shibata (1996) did not predict the mass of the resulting accretion torus except to assume that it vanishes when the radius of tidal disruption is less than that of the ISCO. A parallel systematic study has been pursued recently to exploit the relativistic *"affine-model"* and to describe the properties of the tidally deformed NS (Ferrari et al. 2009, 2010). Also in this case, however, the study did not make any prediction on the final outcome of the merger since it concentrated on the evolution of stationary configurations.

In this paper, we attempt to bridge the gap between intensive numerical simulations and semi-analytical studies by establishing a way to estimate the mass of the resulting torus. We do this by taking the concept of the tidal disruption to its logical extreme. In other words, we model the NS in the binary as a relativistic tri-axial ellipsoid which is tidally distorted as it orbits in the tidal field of a rotating BH. When the tidal-disruption radius is reached, however, we assume the star to be composed of a system of non-interacting "fluid particles" which move on the corresponding geodesics. We therefore compute the mass of the torus as the integral of the masses of the particles which do not fall into the BH. This clearly represents only a *"toy model"* for the complex dynamics of the merger process, but we show that, with a suitable tuning, it allows us to reproduce with good precision the large majority of the results obtained so far from more accurate but also considerably more expensive numerical-relativity calculations. Most importantly, however, it provides a simple tool to better understand the complex dynamics of the tidal disruption and to cover at once the full space of parameters.

The structure of the paper is as follows. In Section 2, we describe the particular tidal model we use and then how we estimate the mass of the accretion torus. In Section 3, we show that by tuning the free parameter in our model we can reproduce results obtained within fully general-relativistic simulations, thus proving that the tool we build is solid. In Section 4, we present the results of our estimates, leaving an intuitive interpretation of the results and the conclusive overview to Sections 5 and 6, respectively.

2. METHOD

To model the behavior of the NS during the final stages of the inspiral of the mixed binary and before it merges with the BH, we use the improved version of the affine model presented in detail in Ferrari et al. (2009). An important difference with respect to that work is that we do not consider the prescriptions of the quasi-equilibrium approximation and, rather, follow the dynamics of the NS until it is disrupted by the BH tidal field. Furthermore, as mentioned in the introduction, in addition to treating the NS as a tri-axial ellipsoid, we also decompose it into a large number of representative "fluid particles," the kinematic properties of which will be used to study the motion of the NS matter after the tidal disruption. Our toy model is therefore composed of three logical parts: (1) the evolution of the NS deformation as it inspirals toward the BH, (2) the modeling of the tidal disruption, and (3) the calculation of the mass building-up the torus. Each of these parts will be discussed separately in the remainder of this section.

2.1. Neutron Star Deformation—The Affine Model

The idea of modeling stars as ellipsoids has a long history and a thorough analysis of incompressible ellipsoidal figures of equilibrium was performed by Chandrasekhar (1969). When modeling the NS deformation, we are addressing what is known as the compressible Roche–Riemann problem, in which one studies the behavior of a compressible ellipsoid with uniform vorticity parallel to its rotation axis, orbiting a point mass or a rigid sphere. More specifically, we will be using an improved version of the affine model, developed in the 1980s by Carter, Luminet, and Marck to describe the encounters between a BH and a Newtonian star (Carter & Luminet 1982, 1983, 1985; Luminet & Marck 1985; Luminet & Carter 1986) and then applied to BH–NS binaries at the very end of the 1990s (Wiggins & Lai 2000). More recently, in fact, the Newtonian treatment of the star was upgraded to achieve a better description of the NS in mixed compact binaries (Ferrari et al. 2009, 2010). The essential features and assumptions of the improved affine approach used herein may be summarized as follows:

1. the equilibrium structure of the NS is determined by the Tolman–Oppenheimer–Volkoff (TOV) equations, while its dynamical behavior is governed by Newtonian hydrodynamics improved by the use of an effective relativistic scalar potential (Rampp & Janka 2002);
2. the NS center of mass moves in the tidal field of a Kerr BH along a simple inspiralling equatorial orbit (cf. Equation (21)) and each point of the orbit is associated with a BH timelike circular geodesic;
3. throughout the inspiral, the NS remains a Riemann S-type ellipsoid, i.e., its spin and vorticity are always parallel and their ratio is constant (see Chandrasekhar 1969); and
4. tidal effects on the orbital motion and the perturbation induced by the star on the BH are neglected.

For completeness, we next review the mathematical formulation of the affine model used herein by writing the equations governing the NS deformations in the principal frame, i.e., the frame associated with the principal axes of the stellar ellipsoid. In this frame, the fluid variables of the affine model are five: the three principal axes of the stellar ellipsoid a_1, a_2, and a_3, the angular frequency of the internal fluid motion Λ, and the star spin measured in the parallel-transported frame associated with the center of mass of the star Ω (Marck 1983). The axis a_3 is perpendicular to the orbital plane, while a_1 and a_2 are perpendicular to one another and to a_3. In the Newtonian limit ($M_{\rm BH} \ll r$, where $M_{\rm BH}$ is the BH mass and r is the Boyer–Lindquist radial coordinate), a_1 and a_2 belong to the orbital plane (see Figure 1). The dynamics of four of the five fluid variables is then governed by the following set of equations:

$$\ddot{a}_1 = a_1(\Lambda^2+\Omega^2) - 2a_2\Lambda\Omega + \frac{1}{2}\frac{\hat{V}}{\widehat{\mathcal{M}}}R_{\rm NS}^3 a_1 \tilde{A}_1 + \frac{R_{\rm NS}^2}{\widehat{\mathcal{M}}}\frac{\Pi}{a_1} - c_{11}a_1, \quad (1)$$

$$\ddot{a}_2 = a_2(\Lambda^2+\Omega^2) - 2a_1\Lambda\Omega + \frac{1}{2}\frac{\hat{V}}{\widehat{\mathcal{M}}}R_{\rm NS}^3 a_2 \tilde{A}_2 + \frac{R_{\rm NS}^2}{\widehat{\mathcal{M}}}\frac{\Pi}{a_2} - c_{22}a_2, \quad (2)$$

$$\ddot{a}_3 = \frac{1}{2}\frac{\hat{V}}{\widehat{\mathcal{M}}}R_{\rm NS}^3 a_3 \tilde{A}_3 + \frac{R_{\rm NS}^2}{\widehat{\mathcal{M}}}\frac{\Pi}{a_3} - c_{33}a_3, \quad (3)$$

$$\dot{J}_s = \frac{\widehat{\mathcal{M}}}{R_{\rm NS}^2} c_{12}\left(a_2^2 - a_1^2\right), \tag{4}$$

where the dots denote derivatives with respect to the proper time at the stellar center τ, the c_{ij} denote the components of the BH tidal tensor in the principal frame, $R_{\rm NS}$ is the NS radius, and the index symbols $\tilde{A}_i$ are defined as[3]

$$\tilde{A}_i \equiv \int_0^\infty \frac{d\sigma}{\left(a_i^2+\sigma\right)\sqrt{\left(a_1^2+\sigma\right)\left(a_2^2+\sigma\right)\left(a_3^2+\sigma\right)}}. \tag{5}$$

The effective relativistic self-gravity potential for the isolated NS in spherical equilibrium equilibrium $\widehat{V}$ and the scalar quadrupole moment for the isolated NS in spherical equilibrium $\widehat{\mathcal{M}}$ are given by[4]

$$\widehat{V} \equiv -4\pi \int_0^{R_{\rm NS}} \frac{[\hat{\epsilon}(\hat{r}) + \hat{p}(\hat{r})][m_{\rm TOV}(\hat{r}) + 4\pi \hat{r}^3 \hat{p}(\hat{r})]}{\hat{\rho}(\hat{r})\hat{r}[\hat{r} - 2m_{\rm TOV}(\hat{r})]} \hat{r}^3 \hat{\rho} d\hat{r}, \tag{6}$$

$$\widehat{\mathcal{M}} \equiv \frac{4\pi}{3} \int_0^{R_{\rm NS}} \hat{r}^4 \hat{\rho} d\hat{r} \tag{7}$$

where $\hat{\epsilon}$, $\hat{p}$, and $\hat{\rho}$ are, respectively, the energy density, pressure and rest-mass density distributions at spherical equilibrium and $dm_{\rm TOV}/dr = 4\pi r^2 \epsilon(r)$. The pressure integral Π is calculated as

$$\Pi \equiv \int p(\rho) d^3x = 4\pi \frac{a_1 a_2 a_3}{R_{\rm NS}^3} \int_0^{R_{\rm NS}} p\left(\frac{\hat{\rho}}{a_1 a_2 a_3}\right) \hat{r}^2 d\hat{r}, \tag{8}$$

while

$$J_s \equiv \frac{\widehat{\mathcal{M}}}{R_{\rm NS}^2}[(a_1^2 + a_2^2)\Omega - 2a_1 a_2 \Lambda] \tag{9}$$

is the spin angular momentum of the star. The fifth fluid variable may be expressed in terms of

$$\mathcal{C} \equiv \frac{\widehat{\mathcal{M}}}{R_{\rm NS}^2}\left[\left(a_1^2 + a_2^2\right)\Lambda - 2a_1 a_2 \Omega\right], \tag{10}$$

which is proportional to the circulation in the locally nonrotating inertial frame. We note that because we work in the absence of viscosity, the circulation of the fluid is conserved, i.e., $\dot{\mathcal{C}} = 0$. For simplicity, but also because this is the assumption made by all numerical-relativity simulations to date, we set $\mathcal{C} = 0$ initially (the NS fluid is thus irrotational) so that Equation (10) reduces to

$$\Lambda = \frac{2a_1 a_2 \Omega}{a_1^2 + a_2^2}. \tag{11}$$

The components of the tidal tensor for a Kerr spacetime, expressed in the NS principal frame, are

[3] The $\tilde{A}_i$ are related to the dimensionless index coefficients defined in Chandrasekhar (1969) by the simple dimensional rescaling $A_i = R_{\rm NS}^3 \tilde{A}_i$. In essence, they express the derivative of the self-gravity of the deformed star with respect to its ith axis.

[4] Hats (ˆ) denote quantities calculated for an isolated nonrotating NS at equilibrium.

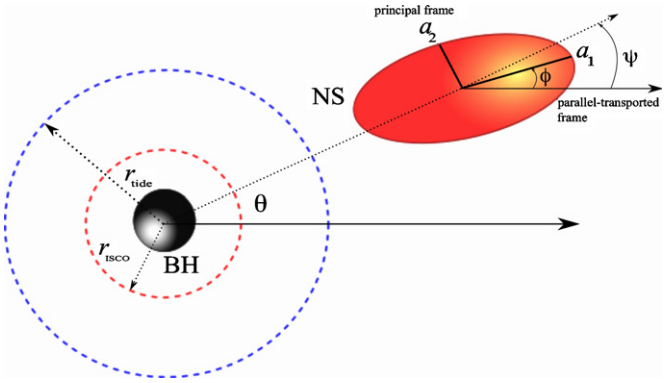

Figure 1. Schematic representation of the toy model. Indicated are the tidal radius $r_{\rm tide}$, the ISCO $r_{\rm ISCO}$, two of the principal axes a_1, a_2, the principal frame, and the parallel-transported frame. Note that for simplicity we set $\phi = \Psi$.
(A color version of this figure is available in the online journal.)

$$c_{11} = \frac{M_{\rm BH}}{r^3}\left[1 - 3\frac{r^2+K}{r^2}\cos^2(\Psi - \phi)\right], \tag{12}$$

$$c_{22} = \frac{M_{\rm BH}}{r^3}\left[1 - 3\frac{r^2+K}{r^2}\sin^2(\Psi - \phi)\right], \tag{13}$$

$$c_{12} = c_{21} = \frac{M_{\rm BH}}{r^3}\left[-\frac{3}{2}\frac{r^2+K}{r^2}\sin 2(\Psi - \phi)\right], \tag{14}$$

$$c_{33} = \frac{M_{\rm BH}}{r^3}\left(1 + 3\frac{K}{r^2}\right), \tag{15}$$

where the angle ϕ (which is related to Ω by $\dot{\phi} \equiv \Omega$) is the angle that brings the parallel-transported frame into the principal frame by a rotation around the a_3 axis (Marck 1983). Similarly, Ψ is an angle that governs the rotation of the parallel-transported tetrad frame in order to preserve the parallel transport of its basis vectors. Stated differently, the difference between Ψ and ϕ represents the lag angle between the principal frame and the parallel transported one, i.e., $\phi_{\rm lag} \equiv \Psi - \phi$, and thus measures how much the star is "lagging behind" in its orbit around the BH. If $\phi_{\rm lag} = 0$, and thus $\Psi = \phi$, then the largest semi-major axis of the star is always pointing toward the BH. A schematic diagram of the BH–NS binary and of the relevant quantities discussed so far is shown in Figure 1.

The constant K appearing in the tidal-tensor components (12)–(15) is a combination of the energy E and the z-orbital angular momentum per unit mass of the star L_z

$$K \equiv (\tilde{a}E - L_z)^2, \tag{16}$$

where $\tilde{a} \equiv J/M$ is the spin of the BH and, for circular geodesics,

$$E \equiv \frac{r^2 - 2rM_{\rm BH} + \tilde{a}\sqrt{rM_{\rm BH}}}{r\sqrt{r^2 - 3rM_{\rm BH} + 2\tilde{a}\sqrt{rM_{\rm BH}}}}, \tag{17}$$

$$L_z \equiv \frac{\sqrt{rM_{\rm BH}}(r^2 - 2\tilde{a}\sqrt{rM_{\rm BH}} + \tilde{a}^2)}{r\sqrt{r^2 - 3rM_{\rm BH} + 2\tilde{a}\sqrt{rM_{\rm BH}}}}. \tag{18}$$

Note that because the tidal-tensor components c_{11} and c_{22} have different signs, the forces acting on the corresponding semi-major axes a_1 and a_2 also have opposite signs and thus lead to a stretching of a_1 and to a compression of a_2.

For simplicity, and to obtain a better agreement with the results of numerical-relativity simulations, we will set hereafter $\phi_{\rm lag} = 0$ and thus $\phi = \Psi$. Furthermore, since we will consider a sequence of circular equatorial geodesics, the radii of which reduce due to the emission of gravitational radiation, the evolution of the angle Ψ is given by (Marck 1983)

$$\dot{\Psi} = \sqrt{\frac{M_{\rm BH}}{r^3}}, \tag{19}$$

and thus also

$$\dot{\phi} = \Omega = \sqrt{\frac{M_{\rm BH}}{r^3}}. \tag{20}$$

In order to evolve the equations of the affine model (1)–(3) we must select an EOS for the NS matter and specify the initial conditions and the evolution of the orbit. As far as the first is concerned, the model is sufficiently general that any EOS could be used and indeed several different ones were used in Ferrari et al. (2010). However, because here we want to compare with the results of numerical-relativity simulations and these have been performed mostly with a Γ law EOS $p = (\Gamma - 1)\rho\epsilon$ which for the adiabatic process considered in this paper is equivalent to a polytropic EOS $p = K\rho^\Gamma$ with $\Gamma = 2$ or 2.75, we will consider here just polytropes with these polytropic exponents and present the result of more realistic EOSs in a subsequent work. As for the initial conditions, we consider an initial separation for the binary, $r_0 \equiv r(t = 0)$, and set $\phi_0 \equiv \phi(t = 0) = 0$, while Ω and Λ are automatically given by Equations (20) and (11), respectively. For the NS axes, instead, we set the time derivatives on the left-hand sides of Equations (1)–(3) to zero and solve the system for a_1, a_2, a_3 with a Newton–Raphson scheme. Of course, it is necessary to ensure that r_0 is large enough, i.e., that initially $a_1 \simeq a_2 \simeq a_3 \simeq R_{\rm NS}$ and $J_s \simeq 0$ (as well as $\mathcal{C} = 0$), and that the final results are unchanged if one chooses a larger r_0. In other words, at $t = 0$ the NS must almost be at spherical equilibrium and the calculations must therefore be independent of the specific choice made for r_0.

For the time evolution of the orbital separation r, we consider a very simple circular equatorial adiabatic inspiral (Misner et al. 1973), which accounts therefore for the radiative losses of two point masses at a 2.5 post-Newtonian (PN) approximation

$$r(t) = r_0 \left(1 - \frac{t}{t_c}\right)^{1/4}, \tag{21}$$

where

$$t_c = \left(\frac{5}{256}\right) \frac{r_0^4}{M_{\rm NS} M_{\rm BH}(M_{\rm NS} + M_{\rm BH})} \tag{22}$$

is the inspiral time and $M_{\rm NS}$ is the gravitational mass of the NS. When generating the orbit, we evolve the orbit angle θ according to the Kerr spacetime equation

$$\frac{d\theta}{dt} = \frac{1}{\tilde{a} + \sqrt{r^3/M_{\rm BH}}} \tag{23}$$

and we make the following approximation, setting

$$\frac{d\tau}{dt} = 1. \tag{24}$$

It is important to remark that our goal is that of computing the mass of the torus produced by the tidal disruption and not that of providing an accurate description of the binary inspiral. In this sense, using a lower-order PN description of the orbit is very reasonable as the dynamics we are most interested in take place when the presently available PN models are no longer accurate.

Once the orbit is determined, we may integrate the affine-model equations, terminating the evolution when the ratio of the semi-major axes a_2 and a_1 reaches a critical value $(a_2/a_1)_{\rm crit}$. This quantity cannot be determined a priori and is effectively a free parameter in our toy model. However, it may be tuned by comparing the results of the toy model with those of the numerical simulations and the way we do this will be discussed in the next section. We thus define the tidal-disruption radius $r_{\rm tide}$ as the orbital separation at which $(a_2/a_1) = (a_2/a_1)_{\rm crit}$.

A final quantity which is relevant to introduce and that may be useful to interpret the results of the toy model is the ISCO, which, for a generic Kerr BH is given by (Bardeen et al. 1972)

$$r_{\rm ISCO} = M_{\rm BH}\{3 + Z_2 \mp [(3 - Z_1)(3 + Z_1 + 2Z_2)]^{1/2}\},$$

$$Z_1 = 1 + (1 - \tilde{a}^2/M_{\rm BH}^2)^{1/3}[(1 + \tilde{a}/M_{\rm BH})^{1/3} + (1 - \tilde{a}/M_{\rm BH})^{1/3}],$$

$$Z_2 = (3\tilde{a}^2/M_{\rm BH}^2 + Z_1^2)^{1/2} \tag{25}$$

where the upper/lower sign holds for co-rotating/counter-rotating orbits. In general, the ISCO is inside the tidal radius, i.e., $r_{\rm ISCO} < r_{\rm tide}$, but there are situations in which the opposite is true and this is the case, for instance, when considering binary systems with very small mass ratios or stars with very large compactness. In these cases too, we follow the evolution of the axis ratio and "disrupt" the NS inside the ISCO as soon as the critical value is reached.

2.2. Neutron Star Disruption

As mentioned above, when the affine-model evolution of the mixed binary leads to the tidal disruption of the NS, we fragment the NS into fiducial fluid elements that would be representative of the motion of the NS matter. The first step in our strategy consists therefore in switching from the five fluid variables of the affine-model formulation to a description of the (disrupted) NS fluid as a set of test particles, each one of which possesses a mass, a 4-position, and a 4-velocity. In practice, at disruption we build a fine grid adapted to the ellipsoidal shape of the star and divide the star into a collection of fluid elements. In the principal frame, the center of each fluid element is identified by a 3-vector $\vec{x}$ and we calculate the mass of the corresponding fluid cell by multiplying the mass density at its center by the volume of the fluid element. Moreover, we may associate with the center of mass of each cell a 3-velocity, which, in the principal-axes frame, is given by (Chandrasekhar 1969)

$$\vec{u} = \vec{u}_s + \vec{u}_e, \tag{26}$$

where

$$\vec{u}_s \equiv \frac{a_1}{a_2}\Lambda x_2 \vec{e}_1 - \frac{a_2}{a_1}\Lambda x_1 \vec{e}_2 \tag{27}$$

is the spin velocity (i.e., the speed of the fluid due to its rotation), and

$$\vec{u}_e \equiv \frac{\dot{a}_1}{a_1} x_1 \vec{e}_1 + \frac{\dot{a}_2}{a_2} x_2 \vec{e}_2 + \frac{\dot{a}_3}{a_3} x_3 \vec{e}_3 \tag{28}$$

is the ellipsoid expansion/contraction velocity, $\vec{e}_i$ being the unit vectors along the ellipsoid principal axis a_i. The coordinate x_i along the ith axis runs from $-a_i$ to a_i. With a rotation of an angle ϕ around a_3, we switch from position 3-vectors in the principal frame to position 3-vectors in the parallel-transported tetrad associated with the NS center of mass, where the 3-velocity $\vec{u}$ becomes $\vec{u} + \vec{\Omega} \times \vec{x}$. In this parallel-transported tetrad, the time component of the position vectors is simply $x^{(0)} = 0$ and we determine the time component of each 4-velocity vector by exploiting the normalization condition $u^{(\alpha)} u_{(\alpha)} = -1$. Finally, we express all the 4-position and the 4-velocity vectors in Boyer–Lindquist coordinates by applying the transformation laws derived in Marck (1983) and summarized in the Appendix.

The procedure described above provides a complete description, in Boyer–Lindquist coordinates, of the kinematic properties of fluid parcels as point particles freely falling in a Kerr spacetime; this is what is needed to then estimate the torus mass.

2.3. Torus Mass Estimation

When looking carefully, in numerical-relativity simulations, at the dynamics of the NS after it is disrupted, it is quite striking to note how much the different parts of the star seem to behave like independent freely falling particles: the gravity of the BH alone does seem to represent the dominant force at this stage of the evolution. In view of this observation, when the NS is tidally disrupted and split into fiducial fluid elements of which we know the mass, the 4-position, and the 4-velocity, we assume that the pressure gradients across neighboring elements and the self-gravity of the system play little role, and hence that the fluid elements behave as independent collisionless fluid particles. As such, after the disruption the NS is approximated as an ensemble of about 3.1×10^4 fluid particles which have a complex distribution of energy and angular momenta, but are in free-fall toward the BH.

Using the 4-velocity of each particle, we compute the corresponding conserved quantities by inverting the relations

$$\frac{dt}{d\tau} = \frac{-\tilde{a}(\tilde{a} e \sin^2\theta - \ell_z) + (r^2 + \tilde{a}^2) P/\Delta}{r^2 + \tilde{a}^2 \cos^2\theta}, \tag{29}$$

$$\left(\frac{dr}{d\tau}\right)^2 = \frac{P^2 - \Delta[r^2 + (\ell_z - \tilde{a} e)^2 + \mathcal{Q}]}{(r^2 + \tilde{a}^2 \cos^2\theta)^2}, \tag{30}$$

$$\left(\frac{d\theta}{d\tau}\right)^2 = \frac{\mathcal{Q} - \cos^2\theta[\tilde{a}^2(1 - e^2) + \ell_z^2/\sin^2\theta]}{(r^2 + \tilde{a}^2 \cos^2\theta)^2}, \tag{31}$$

$$\frac{d\phi}{d\tau} = \frac{-(\tilde{a} e - \ell_z/\sin^2\theta) + \tilde{a} P/\Delta}{r^2 + \tilde{a}^2 \cos^2\theta}, \tag{32}$$

where

$$P \equiv e(r^2 + \tilde{a}^2) - \ell_z \tilde{a}, \tag{33}$$

$$\Delta \equiv r^2 - 2 r M_{\rm BH} + \tilde{a}^2, \tag{34}$$

and e, ℓ_z, and $\mathcal{Q}$ represent the energy, angular momentum, and Carter's constant of motion, respectively, all normalized to the mass of the particle. Note that it is necessary to use these general equations instead of Equations (17) and (18) as the majority of the particles no longer follows circular equatorial geodesics.

As mentioned previously, we identify the mass of the remnant torus with the sum of the masses of the bound particles and we make use of Equation (30) to determine whether a given particle is bound or not. Noting that a turning point occurs when $(dr/d\tau)^2$ passes through zero and since the only influence of θ is to decrease the overall magnitude of $(dr/d\tau)^2$ but not to change its sign, we only consider, without loss of generality, the case $\theta = \pi/2$. We then use root-finding techniques for each particle and consider bound those particles for which $(dr/d\tau)^2 < 0$ at a radial position $r_{\rm TP}$ outside the event horizon $r_{\rm EH}$, such that $r_{\rm EH} < r_{\rm TP} < r_{\rm tide}$ (note that $(dr/d\tau)^2$ is always greater than 0 at $r = r_{\rm tide}$) and simultaneously satisfy $e < 1$. This final condition merely states that the gravitational binding energy has compensated the kinetic energy such that the total energy of the particle is less than the rest mass of the particle at infinity.

Once the NS is tidally disrupted, the calculation of the torus mass, which is initially set to be $M_{\rm b,tor} = M_{\rm b,NS}$, is done as follows.

1. For each fluid particle we verify whether it is bound or not. In this latter case, we assume the particle will accrete onto the BH.[5]
2. The composite mass of the accreted particles is added to the mass of the BH and the mass of the torus is decreased by the corresponding amount.
3. We reconsider the remaining particles and verify if they are still bound or if they would now accrete onto the new and more massive BH.

This procedure is repeated until there are no more particles that would accrete onto the BH or, equivalently, until the relative change in the mass of the torus is less than one part in one million.

In addition to a change in the mass of the BH, we have also experimented with changing the spin of the BH as a result of the angular momentum accreted with the particles. However, the results in this case are much less robust (the mass of the torus is not a monotonic function of the parameters) and this is probably due to the more complex dependence of the geodesic motion on the spin of the BH, which conflicts with the approximations made here. As a result, we keep the BH spin to be the same as the initial one and it is reassuring that this does not spoil the very good agreement with the numerical simulations.

3. TUNING AND VALIDATION OF THE MODEL

In the affine-model approach based on a quasi-equilibrium approximation and discussed in Ferrari et al. (2009), the disruption radius is identified by the condition $[\partial(a_2/a_1)/\partial r]^{-1} = 0$, i.e., as the radial separation at which the axis ratio a_2/a_1 diverges. Although this singular limit is clearly a shortcoming of the assumption of quasi-equilibrium, it is not obvious how to specify the tidal radius in a way which is not arbitrary to some extent. To remove at least in part this degree of arbitrariness, we have decided to tune the tidal radius by carefully analyzing the

[5] We note that all numerical simulations suggest that the amount of matter leaving the central gravitational potential, i.e., that are unbounded but do not fall onto the BH, is extremely small and can thus be neglected here (see Rezzolla et al. 2010).

Table 1
Comparison Between the Remnant Torus Mass Predictions of Fully General-relativistic Simulations and of Our Model with the Critical Value of a_2/a_1 Tuned to 0.44

Reference	EOS (Γ)	C	q	a	$M_{b,\rm tor}/M_{b,\rm NS}$ (Toy Model)	$M_{b,\rm tor}/M_{b,\rm NS}$ (Simulations)	Error (%)
Tonita et al. (2010)	2.00	0.100	1/5	0.00	0.17	0.17	0
Tonita et al. (2010)	2.00	0.125	1/5	0.00	0.06	0.06	0
Tonita et al. (2010)	2.00	0.145	1/5	0.00	< 0.01	< 0.01	0
Tonita et al. (2010)	2.00	0.150	1/5	0.00	< 0.01	< 0.01	0
Duez et al. (2010)	2.00	0.144	1/3	0.50	0.08	0.08	0
Duez et al. (2010)	2.75	0.146	1/3	0.50	0.11	0.13	18
Duez et al. (2010)	2.75	0.173	1/3	0.50	0.04	0.02	50
Etienne et al. (2009)	2.00	0.145	1/3	0.00	0.02	0.04	100
Etienne et al. (2009)	2.00	0.145	1/3	0.75	0.18	0.15	17
Etienne et al. (2009)	2.00	0.145	1/3	−0.50	< 0.01	< 0.01	0
Etienne et al. (2009)	2.00	0.145	1/5	0.00	< 0.01	< 0.01	0
Shibata et al. (2009)	2.00	0.145	1/3	0.00	0.02	< 0.01	100
Shibata et al. (2009)	2.00	0.160	1/3	0.00	< 0.01	< 0.01	0
Shibata et al. (2009)	2.00	0.178	1/3	0.00	< 0.01	< 0.01	0
Shibata et al. (2009)	2.00	0.145	1/4	0.00	0.01	< 0.01	100
Shibata et al. (2009)	2.00	0.145	1/5	0.00	< 0.01	< 0.01	0

Notes. In the four sections of the table, we examine the results recently provided in (from top to bottom) Tonita et al. (2010), Duez et al. (2010), Etienne et al. (2009), and Shibata et al. (2009). The first four columns of the table following the bibliographic references are the parameters of each BH–NS binary, i.e., the adiabatic index Γ of the NS EOS, the NS compactness C, the mass ratio q, and the dimensionless BH spin a. The following three columns provide the remnant torus masses $M_{\rm tor}$ obtained with our model (labeled "Toy Model"), those obtained with fully general-relativistic calculations (labeled "Simulations"), both given in units of the NS baryonic mass $M_{b,\rm NS}$, and the relative error.

results of recent numerical-relativity simulations and in particular those carried out at the AEI (Tonita et al. 2010), for which we have more direct control over the errors. When doing so, we realized that the critical value of the axis ratio $(a_2/a_1)_{\rm crit}$ is a robust measure across our simulations, but also when comparing with the simulations published in the literature. Hence, we have decided to consider the critical axis ratio $(a_2/a_1)_{\rm crit}$ as a free parameter and to identify its value as the one which allows us to best reproduce the numerical data available.

More specifically, for those initial data for which numerical simulations have been performed, we tuned the free parameter $(a_2/a_1)_{\rm crit}$, within the toy model, so as to minimize the difference between the toy model torus mass predictions and the corresponding numerical-relativity ones. As a result of this procedure we obtain $(a_2/a_1)_{\rm crit} = 0.44$ which is robust across all of the simulations and thus define the tidal radius as the orbital separation at which (a_2/a_1) attains such a critical value. It is reasonable to expect that $(a_2/a_1)_{\rm crit}$ will depend on the BH spin and on the mass ratio. Here, however, we assume that such dependence is weak and thus set it to be constant. As we discuss below, even with this crude approximation we can reproduce most of the numerical results with an error which is below $\sim$15%. As an additional note, we stress that although robust (i.e., a single choice fits well all of the available data), the masses of the tori are rather sensitive to the choice for the critical axis ratio. In particular, for the same binary, a change of $\sim$2% in $(a_2/a_1)_{\rm crit}$ (i.e., a change in the last significant figure) may lead to a change in the last significant figure of the estimated torus mass, and thus up to a $\sim$50% change for cases with a very small remnant mass. This effect disappears if one tunes $(a_2/a_1)_{\rm crit}$ with an extra significant digit.

Before going to the details of the comparison with the numerical simulations it is worth making two remarks. The first one is that after having identified in the axis ratio a consistent parameter which we constrain to the second significant figure, we also expect that it will be further refined as new and more accurate results from numerical simulations become available. The second one has already been made in the introduction and stresses the fact that the numerical data itself do not show a great degree of consistency. While there are two cases which have been considered by more than one group, most of the data available refer to configurations which are slightly different and hence difficult to compare. Even the actual procedure followed to measure the mass of the tori differs from group to group; while most decide to measure the mass at a given time after the formation of the apparent horizon, not all groups use the same time. It would certainly be more reasonable if the measure were performed only when the mass accretion rate has reached a very small and constant value, as was done in Rezzolla et al. (2010), rather than setting a time which may vary from simulation to simulation. Notwithstanding these difficulties, it is remarkable that even for the same configurations (cf. the eighth and the twelfth rows in Table 1), or for some which are not very different (cf. the fifth and ninth rows in Table 1), the numerical results yield tori whose masses differ considerably. Interestingly, the predictions of the toy model are equally distant from the numerical results reported in the eighth and the twelfth rows, thus suggesting that both simulations may be equally imprecise.

Being a toy model, its validity is constrained to within specific ranges of the space of parameters, which we discuss below and which allow us nevertheless to cover essentially all of the complete space of parameters. The first constraint on the range of validity comes from the mass ratio, which cannot be too large since the affine model assumes that the NS inspirals as a test fluid and is therefore increasingly more accurate as the mass

ratio decreases. As a result, we will consider only binaries with mass ratios

$$0.10 \leqslant q \leqslant 0.33.$$

While this condition removes several of the values reported in Shibata et al. (2009), it is not at all unrealistic. We recall, in fact, that the most recent estimates for the mass accreted onto the primary compact object during the common-envelope phase are rather low and thus the BH masses in close BH–NS binaries are likely to fall primarily in values near $M_{\rm BH} \simeq 10\,M_\odot$ (Belczynski et al. 2007). Considering a canonical $1.4\,M_\odot$ NS, BH–NS systems are therefore most likely to come in a mass ratio that is $q \simeq 0.14$.

The second constraint comes from the stellar compactness, which cannot be too small for a relativistic compact star, nor too large given the test-fluid hypothesis of the affine model. As a result, we will consider only binaries where the NS has

$$0.1 \leqslant C \leqslant 0.16.$$

This range covers well the one considered so far in numerical simulations (cf. Table 1), but it is worth remarking that the recent arguments made in Özel et al. (2010) suggest a rather high and generic compactness, $C \sim 0.16$, which is at the edge of the range considered here, and that a standard cold EOS, such as the APR (Akmal et al. 1998) EOS, leads on average to compactnesses $C \sim 0.18$, thus outside of the range considered here. Future simulations in which this EOS is employed will help extend the range of validity in compactness of the toy model.

The third constraint comes from the BH spin, which we cannot take as too large given that we treat the motion of the disrupted NS with geodesics and these would lead to incorrect results if the dimensionless spin parameter $a \equiv J/M_{\rm BH}^2$ is too high (e.g., the ratio $M_{b,\rm tor}/M_{b,\rm NS} \to 1$ for $a \to 1$). As a result, we will consider only binaries where the BH has

$$0.0 \leqslant a \leqslant 0.85.$$

The fourth and final constraint comes from the mass of the torus, for which we need a lower limit. This is even true for numerical simulations, whose precision is not infinite. As a result, we consider the tori to have zero baryonic mass if

$$M_{b,\rm tor} \leqslant 0.01\,M_{b,\rm NS} \simeq 0.014\,M_\odot.$$

The results of the comparison are summarized in Table 1, where, in addition to our numerical simulations (Tonita et al. 2010), we have considered also the data reported in Duez et al. (2010), Etienne et al. (2009), and Shibata et al. (2009). The parameters of each BH–NS binary are reported in the first four columns of the table following the bibliographic references: these are the adiabatic index Γ of the NS EOS, the NS compactness C, the binary mass ratio q, and the initial BH spin a, which does not change from its initial value in our toy model. The last three columns provide, instead, the torus baryonic masses $M_{b,\rm tor}$ obtained with the toy model or with fully general-relativistic calculations (both in units of the NS baryonic mass $M_{b,\rm NS}$), and the relative percentage error.

A rapid inspection of the table, and in particular of its last column, clearly shows that in four cases out of sixteen there are rather large errors, i.e., between 50% and 100%. Not having a clear measure of the error associated with the simulations, it is hard to judge whether this is a limit of the toy model or whether this is a limit of the numerical simulations. It should be remarked, however, that these simulations are those which report tori masses that are close to the limit we consider reasonable (i.e., $M_{b,\rm tor}/M_{b,\rm NS} \simeq 0.01$) and clearly new simulations of those binaries are necessary to settle these differences. However, with the exception of those cases, the table also reveals that the toy model can reproduce the remaining cases (which represent three quarters of the data available) with an error which is at most 18% and is virtually 0 for most of the cases. Considering that the numerical-relativity simulations in Table 1 were performed with different codes and with different initial separations and amounts of eccentricity,[6] we believe that the tuning made for the toy model is both reasonably robust and accurate.

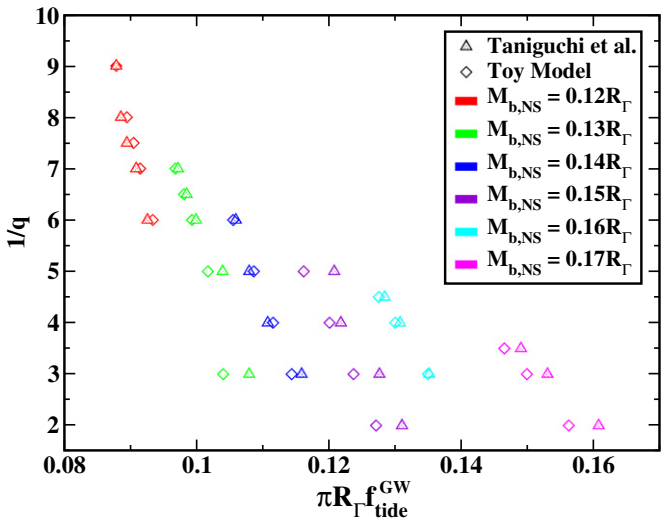

Figure 2. Gravitational-wave frequency at tidal disruption shown as a function of the (inverse of the) mass ratio q (here R_Γ is the polytropic length scale $K^{1/(2\Gamma-2)}$). Data plotted with diamonds are produced with our toy model, while data plotted with triangles are taken from Taniguchi et al. (2008). All neutron stars have $\Gamma = 2$, while their baryonic mass is indicated by the color code in the legend. This figure should be compared with the corresponding Figure 1 in Ferrari et al. (2009).

(A color version of this figure is available in the online journal.)

To further validate the model, we use it to determine the frequency of the gravitational radiation emitted at the onset of the tidal disruption. Results for these frequencies were provided, for example, by Shibata & Taniguchi (2008) and Taniguchi et al. (2008), and we compare to the former in Table 2 and to the latter in Figure 2. The frequencies given in Taniguchi et al. (2008) are found by using quasi-equilibrium sequences of mixed binaries in circular orbits, obtained by solving the Einstein constraint equations in the conformal thin-sandwich decomposition and the relativistic equations of hydrostationary equilibrium; a fitting formula for the frequency is also provided and this is used, in turn, in Shibata & Taniguchi (2008). All cases considered by these authors refer to nonspinning BHs and irrotational NSs, so that, for our model, the gravitational-wave frequency at tidal disruption is given by (cf. Equation (23))

$$f_{\rm tide}^{\rm GW} = \frac{1}{\pi}\sqrt{\frac{M_{\rm BH}}{r_{\rm tide}^3}}, \qquad (35)$$

i.e., by twice the Schwarzschild orbital frequency at the tidal-disruption radius. We note that Figure 2 reports the (inverse of

[6] Although not often discussed, the presence of eccentricity in the initial data can lead to significant changes in the mass of the torus in BH–NS mergers (Tonita et al. 2010).

Table 2
Gravitational-wave Frequency at the Onset of Tidal Disruption $f_{\rm tide}^{\rm GW}$ as Computed with Our Model (Labeled "Toy Model") or as Quoted in Shibata & Taniguchi (2008) (Labeled "Simulations")

q	$M_{b,\rm NS}$	$R_{\rm NS}$	$M_{\rm NS}$	$f_{\rm tide}^{\rm GW}$ (kHz) (Toy Model)	$f_{\rm tide}^{\rm GW}$ (kHz) (Simulations)
0.327	0.15	13.2	1.302	0.856	0.855
0.327	0.16	12.0	1.294	0.997	0.993
0.328	0.14	14.7	1.310	0.736	0.738
0.392	0.15	13.2	1.302	0.877	0.867
0.392	0.16	12.0	1.294	1.021	1.010
0.281	0.15	13.2	1.302	0.840	0.843

Notes. Values in the last columns were calculated in Shibata & Taniguchi (2008) by means of a fitting formula determined in Taniguchi et al. (2008) by using quasi-equilibrium sequences of mixed binaries in circular orbits, obtained by solving the Einstein constraint equations in the conformal thin-sandwich decomposition and the relativistic equations of hydrostationary equilibrium.

the) mass ratio q as a function of $\pi R_\Gamma f_{\rm tide}^{\rm GW}$, where R_Γ is the polytropic length scale $K^{1/(2\Gamma-2)}$. Data plotted with diamonds are produced with our toy model, while data plotted with triangles are taken from Taniguchi et al. (2008). All NSs have $\Gamma = 2$, while their baryonic mass is indicated by the color code in the legend. An inspection of Table 2 and Figure 2 shows that a very good agreement is obtained not only for the torus mass, but also for the gravitational-wave frequency. Stated differently, the assumptions that go into our toy model allow us to accurately capture both the orbital evolution soon *before* the NS disruption takes places and the dynamics of the matter *after* the NS has been disrupted. Moreover, a comparison between our Figure 2 and Figure 1 in Ferrari et al. (2009) shows that the present implementation of the affine model is significantly improved with respect to its quasi-equilibrium formulation.

Before concluding this section, it is important to note that the choice of a critical value for the axis ratio $(a_2/a_1)_{\rm crit}$ also allows us to determine the ratio between the NS self-gravity and the tidal forces. Using a well-known Newtonian argument, when the binary is at the separation $r_{\rm tide}$, the ratio between the tidal and the NS self-gravitational force for a fluid element on the stellar surface when the binary is at the separation $r_{\rm tide}$ is

$$\frac{M_{\rm BH}}{M_{\rm NS}}\left(\frac{a_1}{r_{\rm tide}}\right)^3 = \mathcal{R}, \tag{36}$$

so that when $\mathcal{R} = 1$ the tidal and gravitational forces are equal. Using the affine model and considering the tidal radius as the one at which $a_2/a_1 = (a_2/a_1)_{\rm crit} = 0.44$, we may compute the values of the two forces at tidal disruption. Doing so for the binaries considered in Table 1, we find that $\mathcal{R} \simeq 0.59$–0.70 for the $\Gamma = 2$ cases and $\mathcal{R} \simeq 0.46$–0.47 for the $\Gamma = 2.75$ cases. Our tuning thus reveals that the tidal disruption begins earlier than one would naively think and when the tidal force is only $\sim 1/2$–$1/3$ the self-gravitational one. The tidal force when the binary is at the separation $r_{\rm tide}$ may also be compared to the self-gravitational force of the star at isolation, i.e., when it is a sphere of radius $R_{\rm NS}$. This amounts to calculating the ratio $\mathcal{R}$ when $a_1 \to R_{\rm NS}$, i.e.,

$$\frac{M_{\rm BH}}{M_{\rm NS}}\left(\frac{R_{\rm NS}}{r_{\rm tide}}\right)^3 = \mathcal{R}', \tag{37}$$

and enables us to compare our results with those of Taniguchi et al. (2008), where it was found that $\mathcal{R}' \simeq 0.07$. More specifically, for the binaries considered in Table 1 we find $\mathcal{R}' \simeq 0.08 - 0.11$, which is in good agreement with the aforementioned result. Stated differently, this reveals that the tidal disruption begins when the tidal force is roughly only $\sim 1/10$ of the NS self-gravity at infinite separation.

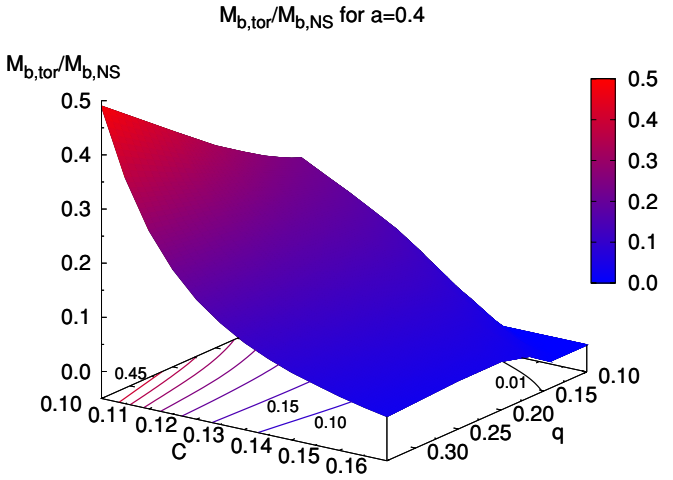

Figure 3. Torus baryonic mass in units of the stellar mass $M_{b,\rm tor}/M_{b,\rm NS}$ shown as a function of the compactness C and of the mass ratio q, for a BH with spin parameter $a = 0.4$.
(A color version of this figure is available in the online journal.)

4. RESULTS

Having tuned and validated the model, we will next consider its predictions for the baryonic mass of the torus as a function of the mass ratio q, the stellar compactness C, and the BH spin parameter a. Because this space of parameters is three dimensional, it is more convenient to consider constant-spin slices and hence we will first comment on a fiducial case of a spinning BH with $a = 0.4$ and then discuss how these results change across the possible values of the spin.

Most of our results are summarized in Figure 3, which shows the baryonic mass of the torus in units of the stellar mass, $M_{b,\rm tor}/M_{b,\rm NS}$, as a function of the stellar compactness C and of the binary mass ratio q, with the data referring to a binary in which the BH has a dimensionless spin parameter $a = 0.4$. Quite clearly, the final mass in the torus varies considerably across the possible space of parameters and is systematically larger the smaller C is. This is rather obvious: the smaller the compactness, the more "Newtonian" the star will be and thus the smaller will the effective gravity at its surface be. In turn, this means that, all else equal, it will be easier to disrupt it even at large distances from the BH (i.e., $r_{\rm tide}$ is comparatively large) and hence to produce a more massive torus.

At the same time, Figure 3 shows that the mass in the torus will be larger when the BH and the NS have comparable masses. Also this result is quite obvious: the smaller the mass ratio, the more unlikely it will be for the star to be tidally disrupted and to be accreted "whole" by the BH. Putting things together, a BH–NS system with a large binary mass ratio and a small NS compactness maximizes the yields in terms of torus mass. For the same reasons, binaries with small mass ratios and large compactnesses will yield the smallest tori. To fix the ideas: for a BH–NS system with $a = 0.4$, the toy model predicts that $M_{b,\rm tor}/M_{b,\rm NS} \sim 0.5$ when $C = 0.10$ and $q = 0.33$, while essentially no tori are produced for $q \lesssim 0.14$ and $C \gtrsim 0.14$ (cf. third panel of Figure 4 where these data are also shown with

contour plots). Overall, our toy model suggests that, at least statistically, a BH with spin larger than $\simeq 0.4$ is necessary to produce any astrophysically relevant torus.

The generic predictions of the toy model for $a = 0.4$ remain unchanged when considering also other BH spins, extending smoothly from smaller to larger spins. This is summarized in Figure 4, the different panels of which refer, from top to bottom, to $a = 0.0, 0.2, 0.4, 0.6, 0.8, 0.85$, respectively. The baryonic mass of the torus is still expressed in units of NS mass and is reported as a function of the NS compactness and of the binary mass ratio, but it is shown by means of contour plots to better quantify the results. The numerical values of some representative contour lines are shown and allow for a direct measurement (the contours are equally spaced in a linear scale), while the thick and black solid line shows the area below which no torus is created (i.e., the "no-torus" area with $M_{b,\rm tor}/M_{b,\rm NS} < 0.01$). Finally, shown with a horizontal dot-dashed line is the most likely mass ratio for a canonical $1.4\,M_\odot$ NS.

Moving from the top to the bottom of Figure 4 it is easy to recognize that the maximum mass attained at the smallest compactness increases significantly with the BH spin, ranging from $M_{b,\rm tor} \simeq 0.18\,M_{b,\rm NS} \simeq 0.25\,M_\odot$ for $a = 0.0$, to $M_{b,\rm tor} \gtrsim 0.95\,M_{b,\rm NS} \simeq 1.33\,M_\odot$ for $a = 0.85$. At the same time, the "no-torus" area decreases and virtually disappears for $a \gtrsim 0.6$. Stated differently, for sufficiently large BH spins a torus is *always* produced and with non-negligible mass. As an example, taking as fiducial compactness the canonical value of $C \simeq 0.145$, the torus mass at the fiducial mass ratio goes from $M_{b,\rm tor} \simeq 0.06\,M_{b,\rm NS} \simeq 0.08\,M_\odot$ for $a = 0.4$, to $M_{b,\rm tor} \simeq 0.24\,M_{b,\rm NS} \simeq 0.34\,M_\odot$ for $a = 0.85$.

A complementary view, because it refers to a different slicing of the space of parameters, is illustrated in Figure 5, which is the same as in Figure 4, but it shows the baryonic mass as a function of the BH spin and of the mass ratio for a fixed compactness $C = 0.145$ (left panel), or as a function of the BH spin and of the compactness for a fixed mass ratio $q = 0.14$ (right panel). Both panels of the figure are rather self-explanatory and underline what has already been discussed above: large tori masses are possible for BHs which are spinning sufficiently rapidly or for NSs which are not very compact (favoring a stiff EOS).

In summary, considering an astrophysically realistic mass ratio $q \simeq 0.14$ and a conservative value of the stellar compactness $C \simeq 0.145$ (we recall that even larger values were recently suggested in Özel et al. 2010), the predictions of the toy model are that the torus mass should be

$$M_{b,\rm tor} \lesssim 0.24\,M_{b,\rm NS} \simeq 0.34\,M_\odot \tag{38}$$

for BH spins $0 \leqslant a \leqslant 0.85$. Such masses are comparable but also smaller than the ones predicted by the analysis of unequal-mass NS–NS mergers carried out by Rezzolla et al. (2010).

5. AN INTUITIVE INTERPRETATION

In the previous section, we have shown that the complex dynamics of the tidal disruption and subsequent accretion onto the BH is well captured by the simple assumptions needed to build our toy model. In what follows, we will show that an even simpler framework can be built to explain at least qualitatively the results of the toy model.

We have already noted that binaries with less compact NSs produce bigger tori as these are more "Newtonian" and hence are capable of sustaining smaller tidal forces before being disrupted. Stated differently, less compact stars have larger tidal radii $r_{\rm tide}$. In the usual arguments this quantity is generally compared to the ISCO, and the standard line of argument says that a BH–NS binary will produce a torus if $r_{\rm tide} \gtrsim r_{\rm ISCO}$. This reasoning, however, is inadequate for systems which yield low mass tori. An obvious failure of the argument is offered by an NS that is disrupted by its BH companion exactly at $r_{\rm tide} = r_{\rm ISCO}$. In this case, half of the star would still be outside the ISCO and thus potentially capable of producing a torus.

The necessary, but not sufficient, condition for a BH–NS binary to yield a torus is thus better expressed as

$$\frac{r_{\rm tide} + a_1(r_{\rm tide}) - r_{\rm ISCO}}{2R_{\rm NS}} \simeq 1 + \frac{r_{\rm tide} - r_{\rm ISCO}}{2R_{\rm NS}} > 0, \tag{39}$$

where the second expression is obtained after recognizing that at tidal disruption $a_1(r_{\rm tide}) \simeq 2R_{\rm NS}$. Expression (39) has three important properties: it is dimensionless, it combines the three fundamental length scales of our system, and it essentially measures how many NS diameters fit between $r_{\rm tide} + a_1(r_{\rm tide})$ and $r_{\rm ISCO}$ (cf. Figure 1). In other words, Equation (39) quantifies "how much useful space" there is for the NS to form a torus after it is tidally disrupted.

At this point, it is natural to associate this quantity directly with the mass of the torus expressed in units of the NS mass

$$\frac{M_{b,\rm tor}}{M_{b,\rm NS}} \propto \left[1 + \frac{r_{\rm tide} - r_{\rm ISCO}}{2R_{\rm NS}}\right], \tag{40}$$

where the exact proportionality will depend (albeit weakly) on q and C. Not surprisingly, Equation (40) reproduces, at least qualitatively, all of the phenomenology discussed before and predicted by our toy model. As an example, for fixed BH mass and spin, and hence fixed $r_{\rm ISCO}$, the torus mass will increase for less compact NSs since for these $r_{\rm tide}$ will grow and more rapidly than $R_{\rm NS}$. Similarly, given a BH, for a fixed NS compactness, and hence for a fixed $R_{\rm NS}$, the torus mass will grow with the BH spin as does the difference $r_{\rm tide} - r_{\rm ISCO}$ ($r_{\rm ISCO}$ decreases more rapidly than $r_{\rm tide}$).

6. CONCLUDING REMARKS

The production of a massive torus orbiting stably around a rotating BH is a necessary ingredient in all models that explain SGRBs in terms of the coalescence of binary systems composed of a BH and an NS or of two NSs. The accurate calculation of this mass inevitably requires the use of numerical-relativity simulations, which, however, are still very expensive and have so far been applied only to a tiny patch of the possible space of parameters. In the case of BH–NS binaries especially, the space of parameters is particularly extended as it involves the mass ratio of the binary q, the stellar compactness C, and the BH spin a. As a result, we presently have only a very limited idea of what are the likely torus masses that this process will yield and hence have a rather limited ability to assess whether or not the merger of a BH–NS system under astrophysically realistic conditions will serve as a robust scenario for the powering of SGRBs.

To compensate for this lack of knowledge, we have developed a toy model that allows for the computation of the mass of the torus without having to perform a numerical-relativity simulation. In essence, we model the NS in the binary as a tri-axial ellipsoid which is tidally distorted as it orbits in the tidal field of a rotating BH and as described by the relativistic affine model. When the star is disrupted, we decompose it into

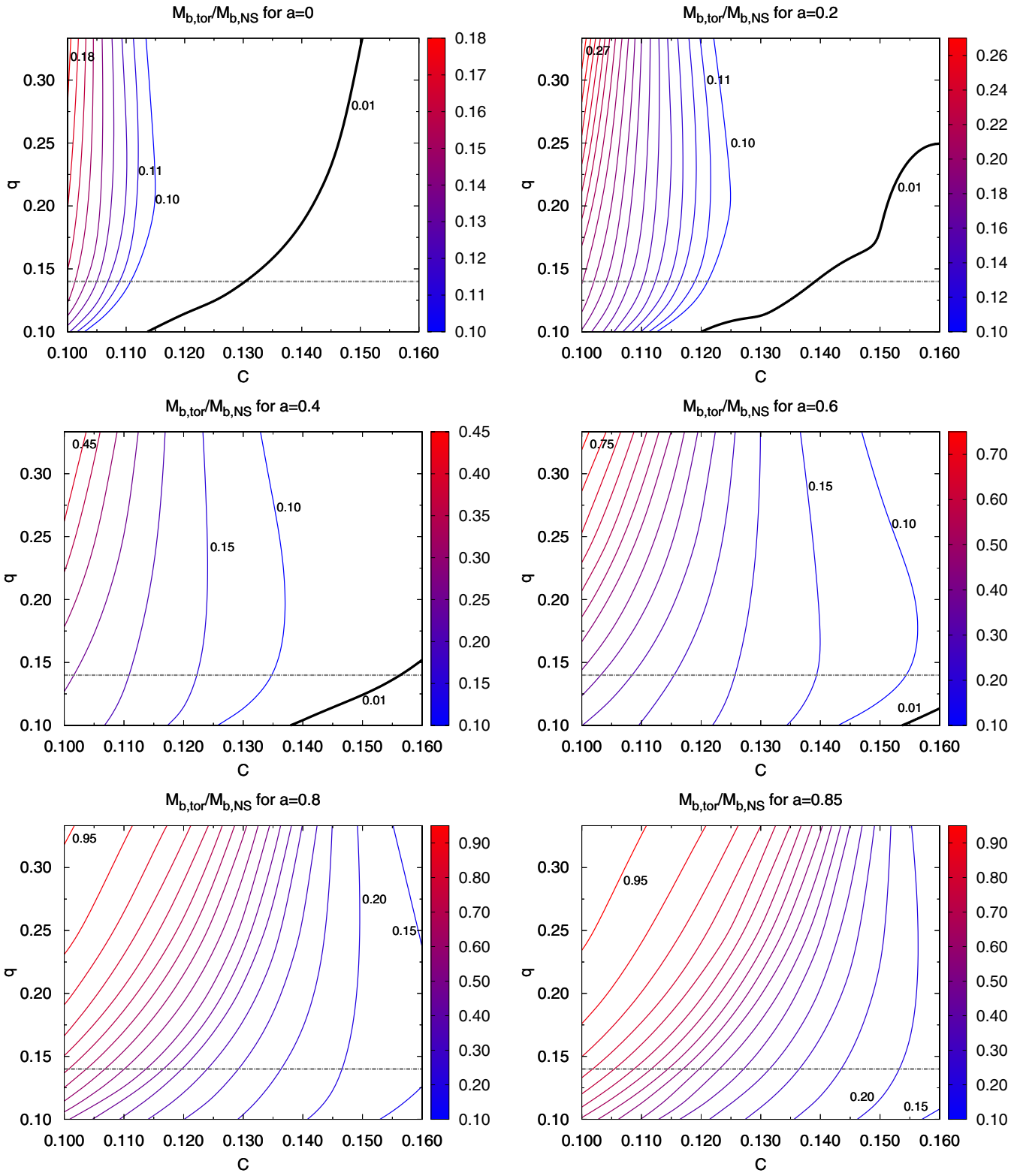

Figure 4. Torus baryonic mass in units of the stellar mass $M_{b,\rm tor}/M_{b,\rm NS}$ shown as a function of the compactness C and of the mass ratio q. From top to bottom, the different panels refer to different values of the BH spin ($a = 0.0, 0.2, 0.4, 0.6, 0.8, 0.85$) and the numbers on the iso-mass contours are used to indicate the constant spacing between two successive contours and the range they span. In each panel, no torus is created below the thick, black, solid line (i.e., this line marks the boundary of the "no-torus" region with $M_{b,\rm tor}/M_{b,\rm NS} < 0.01$), while the horizontal dot-dashed line shows the most-likely binary mass ratio in the case of a canonical $1.4\,M_\odot$ NS.

(A color version of this figure is available in the online journal.)

a system of non-interacting "fluid particles" which move along geodesics. We therefore compute the mass of the torus as the integral of the masses of the particles which do not fall into the BH. The only free parameter in our model is the radius at which

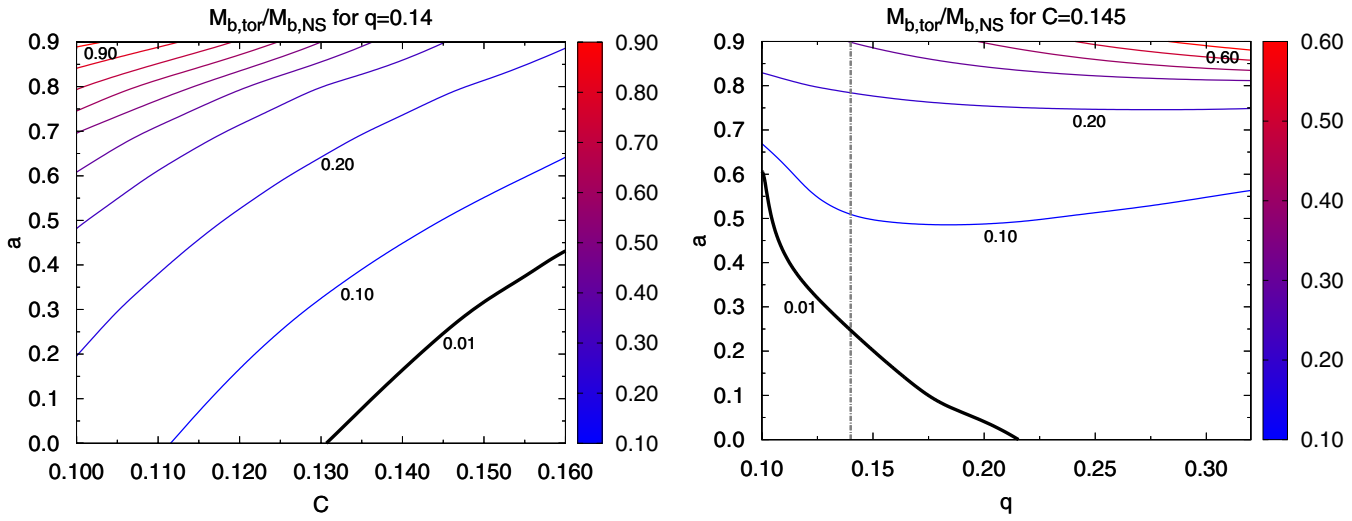

Figure 5. Same as in Figure 4 but considering different slices of the space of parameters. In particular, the torus baryonic mass in units of the stellar mass $M_{b,\rm tor}/M_{b,\rm NS}$ is shown as a function of the BH spin and the NS compactness for $q = 0.14$ (left panel) and as a function of the BH spin and binary mass ratio for $C = 0.145$ (right panel).

(A color version of this figure is available in the online journal.)

the tidal disruption takes place and which we tune in terms of the ratio of the semi-major axes on the equatorial plane and with the aid of numerical-relativity simulations. The tuning requires care, but allows us to reproduce with precision the majority of the available data, some of which shows inconsistencies of their own.

As it is natural for a semi-analytic approach, the model has a limited range of validity, which we have decided to set in the following ranges for the mass ratio, compactness, and BH spin: $0.10 \leqslant q \leqslant 0.33$, $0.1 \leqslant C \leqslant 0.16$, $0.0 \leqslant a \leqslant 0.85$, respectively. Overall, the toy model predicts that high BH spins, small mass ratios, and small NS compactnesses all enhance the mass of the remnant torus. As a result, tori with masses as large as $M_{b,\rm tor} \simeq 1.33\,M_\odot$ are predicted for $q \simeq 0.3$ and for a very extended star, with compactness $C \simeq 0.1$, inspiralling around a BH with dimensionless spin $a = 0.85$. However, when considering a more astrophysically reasonable mass ratio $q \simeq 0.14$ and a conservative but realistic value of the compactness $C \simeq 0.145$, the predictions of the toy model set a considerably smaller upper limit of $M_{b,\rm tor} \lesssim 0.34\,M_\odot$.

All of the phenomenology discussed above has a rather intuitive interpretation and it is easy to show that the torus mass is directly related to how much of the star falls between the tidal radius augmented of the NS semi-major axis and the ISCO. Hence, collecting the three fundamental length scales appearing in the system, the simple expression $M_{b,\rm tor}/M_{b,\rm NS} \propto [1 + (r_{\rm tide} - r_{\rm ISCO})/2R_{\rm NS}]$ is able to capture qualitatively the predictions that our toy model can make quantitatively.

Toy models are by construction approximate representations of much more complex phenomena and their predictions are therefore intrinsically accompanied by errors. Bearing this in mind, the toy model presented here can be further improved as new and more accurate numerical-relativity simulations are performed and as their level of realism increases with the inclusion of microphysical EOSs, magnetic fields, and radiative transfer. This will represent the focus of our future work.

It is a pleasure to thank Bruno Giacomazzo and Jocelyn Read for useful discussions and William Lee and Max Ruffert for their comments. This work was supported in part by the IMPRS on "Gravitational-Wave Astronomy," by the DFG grant SFB/Transregio 7, and by "CompStar," a Research Networking Programme of the European Science Foundation.

APPENDIX

THE PARALLEL-PROPAGATED TETRAD

In this appendix, we gather together the equations derived by Marck (1983) to define a tetrad which is parallel-transported as it moves along a timelike geodesic of a Kerr BH spacetime in Boyer–Lindquist coordinates

$$ds^2 = -\left(1 - \frac{2M_{\rm BH}r}{\Sigma}\right)\mathrm{d}t^2 - \frac{4M_{\rm BH}r}{\Sigma}\tilde{a}\sin^2\theta\,\mathrm{d}t\mathrm{d}\phi + \frac{\Sigma}{\Delta}\mathrm{d}r^2 + \Sigma\mathrm{d}\theta^2 + \frac{\mathcal{A}}{\Sigma}\sin^2\theta\,d\phi^2, \quad \text{(A1)}$$

where

$$\Sigma \equiv r^2 + \tilde{a}^2\cos^2\theta, \quad \text{(A2)}$$

$$\Delta \equiv r^2 + \tilde{a}^2 - 2M_{\rm BH}r, \quad \text{(A3)}$$

$$\mathcal{A} \equiv (r^2 + \tilde{a}^2) - \Delta\tilde{a}^2\sin^2\theta. \quad \text{(A4)}$$

In our model, the test particle is identified with the center of mass of an NS orbiting its rotating BH companion. Marck expresses his results in the canonical symmetric orthonormal tetrad introduced by Carter (1968)

$$\boldsymbol{\omega}^{(0)} = \sqrt{\frac{\Delta}{\Sigma}}(\mathrm{d}t - \tilde{a}\sin^2\theta\mathrm{d}\phi), \quad \text{(A5)}$$

$$\boldsymbol{\omega}^{(1)} = \sqrt{\frac{\Delta}{\Sigma}}\mathrm{d}r, \quad \text{(A6)}$$

$$\boldsymbol{\omega}^{(2)} = \sqrt{\Sigma}\mathrm{d}\theta, \tag{A7}$$

$$\boldsymbol{\omega}^{(3)} = \frac{\sin\theta}{\sqrt{\Sigma}}[\tilde{a}\mathrm{d}t - (r^2+\tilde{a}^2)\mathrm{d}\phi], \tag{A8}$$

which has the convenience of casting the Kerr metric in the form

$$ds^2 = \eta_{(\mu)(\nu)}\boldsymbol{\omega}^{(\mu)}\boldsymbol{\omega}^{(\nu)}, \tag{A9}$$

where $\eta_{(\mu)(\nu)} = \mathrm{diag}(-1,1,1,1)$ is the metric tensor of Minkowksi spacetime. Before expressing the components of the basis vectors of the tetrad found in Marck (1983), we define the quantities α and β

$$\alpha \equiv \sqrt{\frac{K - \tilde{a}^2\cos^2\theta}{r^2+K}}, \tag{A10}$$

$$\beta \equiv \sqrt{\frac{r^2+K}{K-\tilde{a}^2\cos^2\theta}}, \tag{A11}$$

where K is Carter's constant, and the two vectors

$$\tilde{e}_1{}^{(0)} = \alpha\sqrt{\frac{\Sigma}{K\Delta}}r\dot{r}, \tag{A12}$$

$$\tilde{e}_1{}^{(1)} = \frac{\alpha r[E(r^2+\tilde{a}^2) - \tilde{a}L_z]}{\sqrt{K\Sigma\Delta}}, \tag{A13}$$

$$\tilde{e}_1{}^{(2)} = \frac{\beta\tilde{a}\cos\theta(\tilde{a}E\sin\theta - L_z\sin^{-1}\theta)}{\sqrt{K\Sigma}}, \tag{A14}$$

$$\tilde{e}_1{}^{(3)} = \beta\sqrt{\frac{\Sigma}{K}}\tilde{a}\cos\theta\dot{\theta}, \tag{A15}$$

and

$$\tilde{e}_2{}^{(0)} = \frac{\alpha r[E(r^2+\tilde{a}^2) - \tilde{a}L_z]}{\sqrt{\Sigma\Delta}}, \tag{A16}$$

$$\tilde{e}_2{}^{(1)} = \alpha\sqrt{\frac{\Sigma}{\Delta}}\dot{r}, \tag{A17}$$

$$\tilde{e}_2{}^{(2)} = \beta\sqrt{\Sigma}\dot{\theta}, \tag{A18}$$

$$\tilde{e}_2{}^{(3)} = \beta\frac{\tilde{a}E\sin\theta - L_z\sin^{-1}\theta}{\sqrt{\Sigma}}, \tag{A19}$$

where the dots indicate derivatives with respect to the proper time τ, and where E and L_z are, respectively, the energy and the angular momentum about the axis of symmetry of the BH per unit mass of the star. We are now ready to express—in Carter's symmetric tetrad—the components of the vectors forming an orthonormal tetrad parallel-transported along an arbitrary timelike geodesic in a Kerr spacetime. These are

$$e_0{}^{(0)} = \frac{E(r^2+\tilde{a}^2) - \tilde{a}L_z}{\Delta\sqrt{\Sigma}}, \tag{A20}$$

$$e_0{}^{(1)} = \sqrt{\frac{\Delta}{\Sigma}}\dot{r}, \tag{A21}$$

$$e_0{}^{(2)} = \sqrt{\Sigma}\dot{\theta}, \tag{A22}$$

$$e_0{}^{(3)} = \frac{\tilde{a}E\sin\theta - L_z\sin^{-1}\theta}{\sqrt{\Sigma}}, \tag{A23}$$

$$\mathbf{e}_1 = \cos\Psi\tilde{\mathbf{e}}_1 - \sin\Psi\tilde{\mathbf{e}}_2, \tag{A24}$$

$$\mathbf{e}_2 = \sin\Psi\tilde{\mathbf{e}}_1 + \sin\Psi\tilde{\mathbf{e}}_2, \tag{A25}$$

and

$$e_3{}^{(0)} = \sqrt{\frac{\Sigma}{K\Delta}}\tilde{a}\cos\theta\dot{r} \tag{A26}$$

$$e_3{}^{(1)} = \frac{\tilde{a}\cos\theta[E(r^2+\tilde{a}^2) - \tilde{a}L_z]}{\sqrt{K\Sigma\Delta}}, \tag{A27}$$

$$e_3{}^{(2)} = -\frac{r(\tilde{a}E\sin\theta - L_z\sin^{-1}\theta)}{\sqrt{K\Sigma}}, \tag{A28}$$

$$e_3{}^{(3)} = \sqrt{\frac{\Sigma}{K}}r\dot{\theta}. \tag{A29}$$

The rotation by an angle Ψ in Equations (A24) and (A25) ensures that $\mathbf{e}_{(1)}$ and $\mathbf{e}_{(2)}$ are indeed parallel-transported along any Kerr timelike geodesic. Finally, the evolution of the angle Ψ is governed by Equation (19) for circular equatorial orbits.

REFERENCES

Akmal, A., Pandharipande, V. R., & Ravenhall, D. G. 1998, Phys. Rev. C, 58, 1804

Anderson, M., Hirschmann, E. W., Lehner, L., Liebling, S. L., Motl, P. M., Neilsen, D., Palenzuela, C., & Tohline, J. E. 2008a, Phys. Rev. Lett., 100, 191101

Anderson, M., Hirschmann, E. W., Lehner, L., Liebling, S. L., Motl, P. M., Neilsen, D., Palenzuela, C., & Tohline, J. E. 2008b, Phys. Rev. D, 77, 024006

Baiotti, L., Giacomazzo, B., & Rezzolla, L. 2008, Phys. Rev. D, 78, 084033

Baiotti, L., Giacomazzo, B., & Rezzolla, L. 2009, Class. Quantum Grav., 26, 114005

Baiotti, L., Shibata, M., & Yamamoto, T. 2010, Phys. Rev. D, 82, 064015

Bardeen, J. M., Press, W. H., & Teukolsky, S. A. 1972, ApJ, 178, 347

Bauswein, A., Janka, H. T., & Oechslin, R. 2010, Phys. Rev. D, 82, 084043

Belczynski, K., Taam, R. E., Kalogera, V., Rasio, F., & Bulik, T. 2007, ApJ, 662, 504

Carter, B. 1968, Phys. Rev., 174, 1559

Carter, B., & Luminet, J. P. 1982, Nature, 296, 211

Carter, B., & Luminet, J. P. 1983, A&A, 121, 97

Carter, B., & Luminet, J. P. 1985, MNRAS, 212, 23
Chandrasekhar, S. 1969, Ellipsoidal Figures of Equilibrium (revised edition 1987; New Haven, CT: Yale Univ. Press)
Chawla, S., et al. 2010, Phys. Rev. Lett., 105, 111101
Duez, M. D., Foucart, F., Kidder, L. E., Ott, C. D., & Teukolsky, S. A. 2010, Class. Quantum Grav., 27, 114106
Duez, M. D., et al. 2008, Phys. Rev. D, 78, 104015
Etienne, Z. B., Faber, J. A., Liu, Y. T., Shapiro, S. L., Taniguchi, K., & Baumgarte, T. W. 2008, Phys. Rev. D, 77, 084002
Etienne, Z. B., Liu, Y. T., Shapiro, S. L., & Baumgarte, T. W. 2009, Phys. Rev. D, 79, 044024
Ferrari, V., Gualtieri, L., & Pannarale, F. 2009, Class. Quantum Grav., 26, 125004
Ferrari, V., Gualtieri, L., & Pannarale, F. 2010, Phys. Rev. D, 81, 064026
Giacomazzo, B., Rezzolla, L., & Baiotti, L. 2009, MNRAS, 399, L164
Kluzniak, W., & Lee, W. H. 1999, Astrophys. Lett. Commun., 38, 205
Lee, W. H., & Ramirez-Ruiz, E. 2007, New J. Phys., 9, 17
Liu, Y. T., Shapiro, S. L., Etienne, Z. B., & Taniguchi, K. 2008, Phys. Rev. D, 78, 024012
Löffler, F., Rezzolla, L., & Ansorg, M. 2006, Phys. Rev. D, 74, 104018
Luminet, J. P., & Carter, B. 1986, ApJS, 61, 219
Luminet, J. P., & Marck, J. A. 1985, MNRAS, 212, 57
Marck, J. 1983, Proc. R. Soc. A, 385, 431
Misner, C. W., Thorne, K. S., & Wheeler, J. A. 1973, Gravitation (San Francisco, CA: Freeman)
Nakar, E. 2007, Phys. Rep., 442, 166
Oechslin, R., & Janka, H. T. 2007, Phys. Rev. Lett., 99, 121102
Özel, F., Baym, G., & Guver, T. 2010, Phys. Rev. D, 82, 101301
Rampp, M., & Janka, H.-T. 2002, A&A, 396, 361
Rezzolla, L., Baiotti, L., Giacomazzo, B., Link, D., & Font, J.-A. 2010, Class. Quantum Grav., 27, 114105
Rosswog, S. 2005, ApJ, 634, 1202
Ruffert, M., & Janka, H.-T. 2010, A&A, 514, A66
Shibata, M. 1996, Prog. Theor. Phys., 96, 917
Shibata, M., Kyutoku, K., Yamamoto, T., & Taniguchi, K. 2009, Phys. Rev. D, 79, 044030
Shibata, M., & Taniguchi, K. 2008, Phys. Rev. D, 77, 084015
Taniguchi, K., Baumgarte, T. W., Faber, J. A., & Shapiro, S. L. 2008, Phys. Rev. D, 77, 044003
Tonita, A., Rezzolla, L., & Giacomazzo, B. 2010, Phys. Rev. D, in press
Wiggins, P., & Lai, D. 2000, ApJ, 532, 530
Yamamoto, T., Shibata, M., & Taniguchi, K. 2008, Phys. Rev. D, 78, 064054